Asian Journal of Chemistry; Vol. 35, No. 1 (2023), 99-108

ASIAN JOURNAL OF CHEMISTRY

https://doi.org/10.14233/ajchem.2023.26893

Effect of Zr-Nanofiller on Structural and Thermal Properties of PVDF-*co*-HFP Porous Polymer Electrolyte Membranes Doped with Mg^{2+} Ions

N. KUNDANA[1,2], M. VENKATAPATHY[2,*], V. NEERAJA[3], CHANDRA SEKHAR ESPENTI[3], VENKATA RAMANA JEEDI[1] and V. MADHUSUDHANA REDDY[3]

[1]Department of Chemistry, B.V. Raju Institute of Technology, Narsapur-502313, India
[2]Department of Chemistry, Arignar Anna Government Arts College (Affiliated to Bharathidasan University, Tiruchirapalli), Musiri-621211, India
[3]Department of Chemistry, Malla Reddy College of Engineering & Technology, Hyderabad-500100, India

*Corresponding author: E-mail: drvenkatapathy@yahoo.com

Received: 4 October 2022; *Accepted*: 17 November 2022; *Published online*: 27 December 2022; AJC-21085

New poly(vinylidene fluoride-*co*-hexafluoropropylene) (PVDF-*co*-HFP)/ZrO_2-based nanocomposite porous polymer membranes were prepared with doping of magnesium ions using THF as solvent. These membranes were prepared using the solvent casting technique. The optimal nanofiller (0, 2, 4, 6, 8 and 10% Zr nanopowder) was incorporated into the PVDF-*co*-HFP/$MgTf_3$/ZrO_2 and the incorporation of the nanofiller results in an increase in the porosity of the prepared membranes. The structural, morphological and thermal properties of the nanocomposite porous polymer membranes were also investigated. The structural investigation and the identification of functional groups were accomplished using FTIR technique. X-ray diffraction (XRD) analysis was performed to ascertain the phase of polymer membranes and the phase change that happens upon interaction with nanofiller and Mg^{2+} ions. Assessment of the nanocomposite porous polymer membrane's morphology and porous structure was performed using a scanning electron microscope (SEM). DSC analysis was used to evaluate the thermal behaviour of the nanocomposite porous membranes. The electrical and dielectric studies confirmed the structural reformation of the polymer electrolyte materials. It was found that 8% nanofiller is the best conducting composition for maximum ionic conductivity, dielectric constant and Mg^{2+} ion mobility. The incorporation of ZrO_2 nanofiller predominantly increases the number of free ions and mobility of the charge carriers in the composite polymer electrolyte systems.

Keywords: Polymer membranes, Poly(vinylidene fluoride), Hexafluoropropylene, Porosity, Nanofiller.

INTRODUCTION

Since the invention of lithium-ion batteries in the 1870s, numerous electronic mobile gadgets have undergone enormous advancements. Because of their high specific capacity and portability, lithium-ion batteries have been a driving force behind the consistently growing business that produces them. In addition to being used in a growing range of applications, lithium-ion batteries have also been widely embraced by users of high-capacity electrical products. As a consequence, there are now more specifications needed for them to be useful, such as greater voltage, larger capacity, longer cycle life and a better degree of safety [1,2]. As a result, there are now stricter criteria for the components used in lithium-ion batteries. Most of the lithium-ion batteries on the market today are powered by liquid electrolytes. The polyolefin membrane has the potential for heat shrinkage at high temperatures and leakage of the liquid electrolyte, both of which can cause a variety of safety issues throughout the process of using the batteries [2-4].

Lithium secondary batteries and other electrochemical devices are slowly drifting from the use of liquid electrolytes in preference of polymer electrolytes, which do not require the use of any kind of solvent [5]. In addition to their role as an ionic conductor, these polymer electrolytes also play the role of an electrical insulator (or separator) between the positive and negative electrodes. The stability of gel and the impermeability of liquid electrolyte to the host polymer are the two crucial factors to consider when developing a gel electrolyte. Several gel polymer systems have demonstrated improved performance in recent years, *e.g.* polyethylene oxide (PEO) [6], polymethyl methacrylate (PMMA) [7], polyvinylidene fluoride (PVDF) [8], polyacrylonitrile (PAN) [9] and poly-

vinylidene fluoride hexafluoropropylene (PVDF-*co*-HFP) [10]. However, due to the some inherentance in gel polymer system *e.g.* lithium exhibits low compatibility with PAN and PVDF, moreover inspite of having good mechanical strength, PVDF crystallizes easily, which doesn't help it conduct ions well.

Blending is a straightforward and reliable method for improving the conductivity of polymer electrolytes, in addition to their other characteristics. Recent research on mixing polymer electrolytes has mostly focused on polymers like PVDF, PVDF-*co*-HFP, PMMA and PVC [11]. Polymer electrolytes enhance the ionic conductivity and lower the temperature at which the system undergoes its glass transition because of the special interactions between polymers (primarily due to the van der Waals forces and hydrogen bonds), resulting in the better battery system compatibility and a significant reduction in the crystalline region of the battery system [12].

The search for polymer electrolytes that contain Mg^{2+} ions can be interesting not only for the purpose of comprehending the multivalent cationic conductivity mechanism in the polymer, but also the lower cost, as well as the ease with which they can be handled and fabricated into thin film membranes. In this work, PVDF-*co*-HFP)/ZrO_2-based nanocomposite porous polymer membranes doped with Mg^{2+} ions. In this work, poly-(vinylidene fluoride-*co*-hexafluoropropylene) (PVDF-*co*-HFP)/ZrO_2-based nanocomposite porous polymer membranes doped with Mg^{2+} ions were prepared. The effects of different dosage of ZrO_2 nanopowder on the morphology, porosity and physical structures of nanocomposite porous polymer membranes were also investigated. These effects included both the variation and the influence of the nanopowder.

EXPERIMENTAL

The polymer, poly(vinylidene fluoride-*co*-hexafluoropropylene) (PVDF-HFP) was bought from Sigma-Aldrich and dried in an oven at 50 ºC for 4 h. It had an average molecular weight of 4,000,000. Both magnesium trifluoromethane sulfonate ($MgTf_3$) salt and Zr nanopowder with particle sizes smaller than 50 nm were also procured from Sigma-Aldrich and used as such. Tetrahydrofuran (THF) with a purity of 99% as common solvent for the preparation of polymer electrolyte membranes.

Preparation of PVDF-*co*-HFP/$MgTf_3$/ZrO_2 membranes: PVDF-*co*-HFP at 70 ºC; and Zr nanopowder and $MgTf_3$ were dried at 100 ºC under a vacuum for roughly 4 h. Then the solution casting technique was applied to prepare Mg^{2+}-based nanocomposite porous polymer membranes. In brief, an appropriate composition ratio of PVDF-*co*-HFP and $MgTf_3$ dissolved in 50 mL anhydrous THF was to added to different wt.% of Zr nanopowder (0, 2, 4, 6, 8 and 10%). These compositions were stirred vigorously for 30 h at 55 ºC to obtain a homogenous mixture. The prepared mixture was transferred to a Petri plate that had been thoroughly sterilized and coated with Teflon. The PVDF-*co*-HFP/$MgTf_3$/ZrO_2 was poured into Petri dishes under a vacuum to prevent bubbles and the solvent was allowed to evaporate at room temperature.

Characterization techniques: The crystalline structure of PVDF-*co*-HFP/$MgTf_3$/ZrO_2 membranes was determined using X-ray diffractometer (Goniometer Ultima-IV model) operated at 40 kV/30 mA. In order to collect images of the highest possible quality, scanning electron micrographs were taken using an FEI ApreoLoVac equipped with a 200 kV accelerating voltage. For the purpose of investigating the structural confirmation of the manufactured SPEM, Shimadzu 8201 PC Fourier transform infrared (FTIR) spectrophotometer was used. The temperature and cold resistance of PVDF-*co*-HFP/$MgTf_3$/ZrO_2 membranes were analyzed with the differential scanning calorimetry (Shimadzu DSC-60).

RESULTS AND DISCUSSION

XRD studies: As evidenced by XRD results, Zr nanoparticles were successfully encapsulated within a PVDF-*co*-HFP/$MgTf_3$ membrane (Fig. 1). The crystalline peaks of Zr nanoparticles enclosed within the PVDF-*co*-HFP/$MgTf_3$ membrane were clearly visible. The amorphous nature of the PVDF-*co*-HFP/$MgTf_3$ membrane was demonstrated by the appearance of only two peaks before the addition of Zr nanoparticles [13]. When Zr nanoparticles were introduced into the PVDF-*co*-HFP/$MgTf_3$ membrane, new peaks were correlated to the presence of Zr nanoparticles having the coordinates of 28.44º, 37.71º and 40.73º.

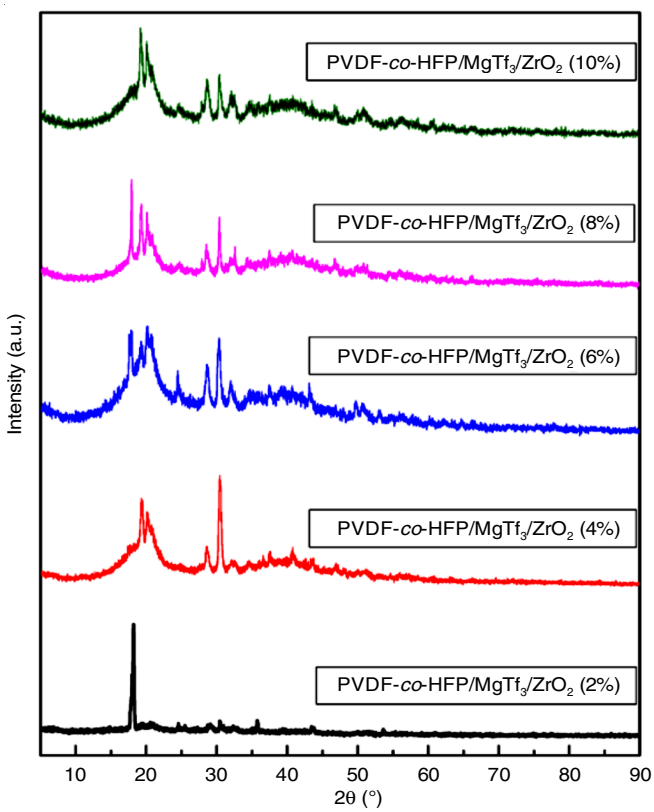

Fig. 1. The XRD peaks of PVDF-*co*-HFP/$MgTf_3$/ZrO_2 with different concentrations of ZrO_2 nanoparticles

As more nanopowder was injected into the membrane, the peak intensity decreased until it reached the level achieved with PVDF-*co*-HFP/$MgTf_3$/ZrO_2 (8% ZrO_2). This indicates that the amorphous nature of the membrane was preserved after it was converted from crystalline to amorphous. This contributes to an increase in the conductivity of the electrolytic membrane [14].

FTIR studies: The inclusion of nanofillers shifts the peak and reduces the absorption peak strength of PVDF polymorphism as observed in Fig. 2. The broadening of the peak from 435 to 400 cm^{-1} with diminished intensity indicates the phase transition. The peak at 400 cm^{-1} may signify -CF_2- wiggling, while the broadening peak in 430-400 cm^{-1} region indicates that anatase phase nano-ZrO_2 vibrations on PVDF-*co*-HFP/$MgTf_3$/ZrO_2 produce a phase transition in PVDF-*co*-HFP. The peak strength of PVDF-*co*-HFP phase observed at 645 cm^{-1}. Observing a shift in frequency from 1109 cm^{-1} to 1085 cm^{-1} reveals a modification in the PVDF-*co*-mixed HFP structure. Moreover, PVDF-*co*-HFP/$MgTf_3$/ZrO_2 is in a complexed state because of its proximity to the F and H atoms [15].

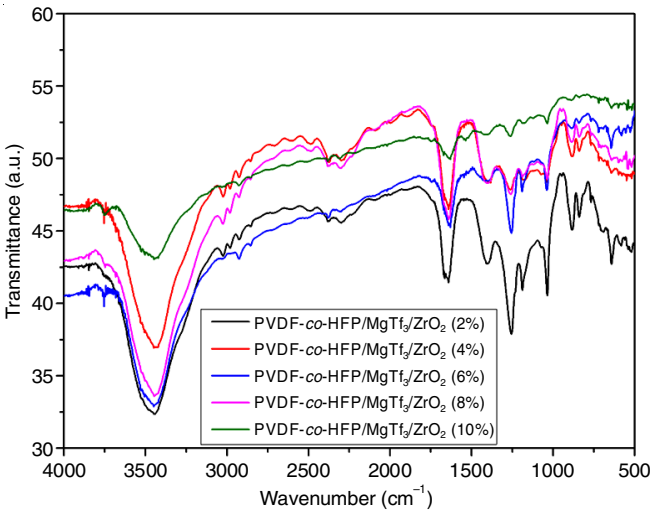

Fig. 2. Illustrates the FTIR peaks of PVDF-*co*-HFP/$MgTf_3$/ZrO_2 with different concentrations of the ZrO_2 nanoparticles

For electronic device applications, the -CF- absorption changes of PVDF-*co*-HFP from 1537 to 1402 cm^{-1} imply -CF- skeletal stretching and an intermediate state of PVDF-*co*-HFP/$MgTf_3$/ZrO_2 (4% ZrO_2). The corresponding peak from 1672 cm^{-1} shifted to 1763 cm^{-1} with the addition of salt, which is attributed to the interaction of Mg^{2+} ion with the -C-F function group of PVDF-*co*-HFP and results in the structural skeletal enlargement of PVDF-*co*-HFP. The interaction between the Mg^{2+} ion and the -CF- functional group of PVDF-*co*-HFP is reduced by the nano ZrO_2 scattered in the polymer electrolyte. The weak intermolecular interactions between the Mg^{2+} ions and the PVDF-co-HFP membrane enable the ions to move freely within the polymer matrix. During this structural transition, the polymer electrolyte enters an amorphous phase, which is beneficial to the nanocomposite polymer electrolyte's high ion mobility [16].

Surface morphological studies: Fig. 3a-e show the surface morphology of produced polymer electrolytes with varied ZrO_2 nanopowder concentrations in PVDF-*co*-HFP/$MgTf_3$. In SEM images depicted in Fig. 3f, nano-powdered ZrO_2 nanoparticles were visible in SEM images. To help in the movement of Mg^{2+} ions more easily, an increase in the concentration of ZrO_2 nanopowder in PVDF-*co*-HFP/$MgTf_3$ has been shown to result in an immense number of fine pores and an increase in the size of the polymer-salt matrix holes. One method is to incorporate HFP groups, which have been shown to improve the mechanical properties of polymer membranes. The PVDF-*co*-HFP/$MgTf_3$ polymer membrane has a rough, granular surface with a few dark micro holes, as seen in Fig. 3a-e, (PVDF-*co*-HFP/$MgTf_3$/$ZrO_2$with different concentrations of ZrO_2 nanoparticles. With varied concentrations of ZrO_2 nanopowder, a shift from semi-crystalline to an amorphous nature on the surface of material

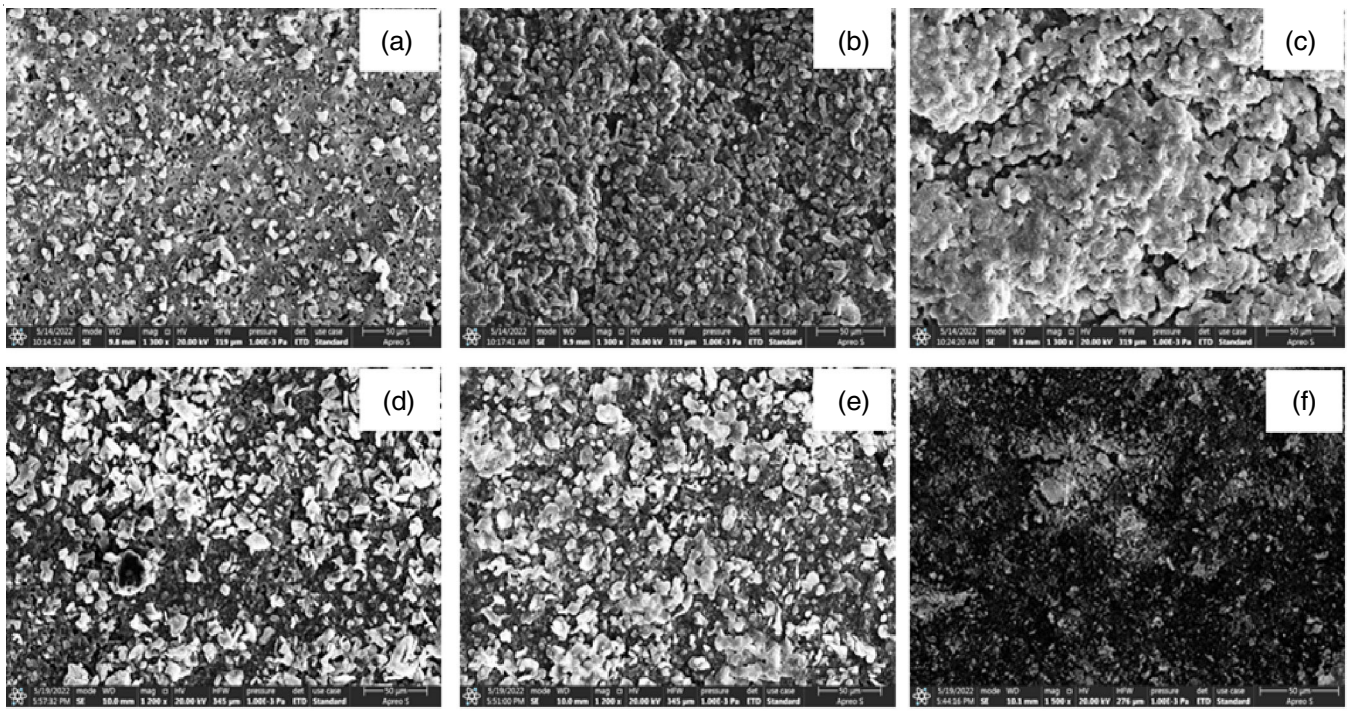

Fig. 3. Illustrates the SEM images of PVDF-*co*-HFP/$MgTf_3$/ZrO_2 (with different concentrations of ZrO_2 nanoparticles) (a-e) and (f) image represents pure ZrO_2 nanoparticles at the magnifications 1300X

was observed. Due to solvent evaporation, the microstructure has holes.

The polymer texture's microporous nature facilitates the movement of Mg^{2+} ions. Solvent and polymer interact in a polymer matrix to create a porous structure that allows solvent to exit the membrane. The microporous interlinking of the matrix facilitates the transport of Mg^{2+} ions. Polymer-salt electrolyte absorption and ion mobility were both facilitated by an increase in the number and size of pores. The monomer units of PVDF-*co*-HFP are responsible for the consistent spherical grain size on the surface of SEM pictures. Mg^{2+} ion interaction with the PVDF-*co*-HFP polymer is indicated by increased pore size and the emergence of a smooth amorphous phase. According to the results, interconnected and massive micropores with smooth surfaces occur at an optimal PVDF-*co*-HFP/$MgTf_3$/ZrO_2 (8% ZrO_2) concentration. This is in support of the amorphous nature, as shown by XRD results.

Differential scanning calorimetry (DSC) studies: Using heating rates of 10 ºC/min and temperatures between 25-200 ºC, the DSC thermograms were generated for PVDF-*co*-HFP/$MgTf_3$ with varied ZrO_2 nanopowder concentrations and are shown in Fig. 4. The melting temperature increases dramatically with increasing ZrO_2 nanopowder concentration [17] and again retained at PVDF-*co*-HFP/$MgTf_3$/ZrO_2 (8% ZrO_2), which might be explained by a change in crystallinity or the local influence of polymer conformation on ZrO_2 nanopowder up to PVDF-*co*-HFP/$MgTf_3$/ZrO_2 (8% ZrO_2) [18]. The T_g and T_m were found to be 87.48 ºC and 124.47 ºC, respectively, for PVDF-*co*-HFP/$MgTf_3$/ZrO_2 (8% ZrO_2). The XRD and SEM images were in agreement with these findings. Because ZrO_2 nanopowder has an amorphous structure, membranes made of PVDF-*co*-HFP/$MgTf_3$ may be better at moving Mg^{2+} ions.

Complex impedance analysis: Electrical impedance spectroscopy (EIS) is the best method for examining the procedure of conducting, transporting and collaboration of nanofiller in the charge carrier development tendency [19]. In this method, nanocomposite polymer electrolyte material *i.e.* PVDF-*co*-HFP/$MgTf_3$/ZrO_2 holding various concentrations of ZrO_2 (2, 4, 6, 8 wt.%) was investigated by placing in between two Ag ion blocking electrodes with a voltage of 20 mV and a frequency of 1Hz-35 MHz was applied. Then the Nyquist plots of real (Z′) *vs.* imaginary (Z″) impedance with different concentration of ZrO_2 at various levels of temperatures is illustrated in Fig. 5a-b, respectively. When the concentration of nanofiller increases the impedance spectrum is shifted towards the starting of *x*-axis (real), *i.e.* for the rise in concentration of nanofiller the mass resistance (R_b) decreasing.

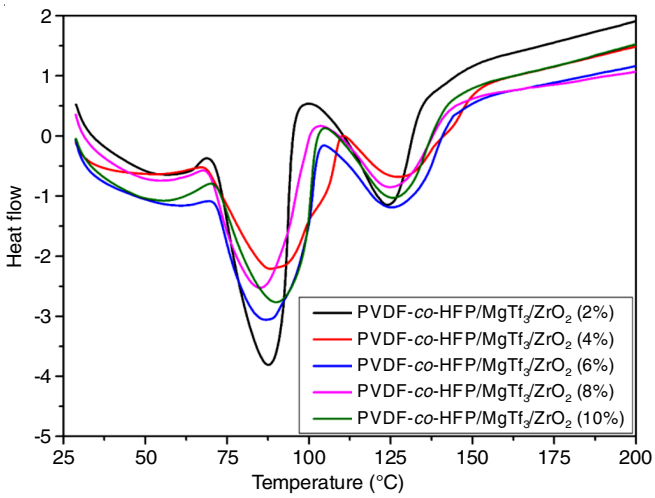

Fig. 4. Illustrates the DSC curves of PVDF-*co*-HFP/$MgTf_3$/$ZrO_2$with various concentrations of the ZrO_2 nanoparticles

All the PVDF-*co*-HFP/$MgTf_3$/ZrO_2 samples shows similar plots that is an enervated semicircle portion at lofty frequency and a spike at low frequency. A semicircle at high frequency depicts (Fig. 5a) the ionic resistance and capacitance of polymer electrolytes, the inclined spikes in the low frequency. Capacitance and resistance increase due to dielectric relaxation and ion trapping and the low frequency spikes are impacted by the charges on the particles (double layer development) at the electrolyte-electrode interface. The low frequency spikes also stipulates the presence of two-layer capacitance at the electrode or sample interface.

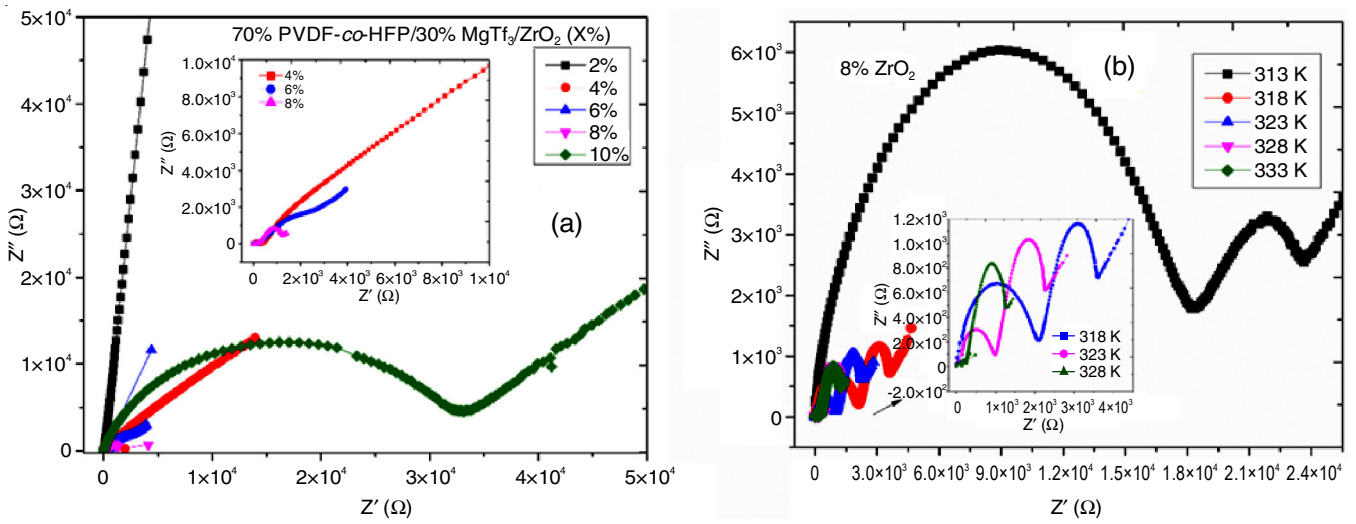

Fig. 5. (a) Cole-Cole plot of PVDF-*co*-HFP/$MgTf_3$/ZrO_2at various concentration and (b) Cole-Cole plot of PVDF-*co*-HFP/$MgTf_3$/ZrO_2(8%) at various temperature

Fig. 6 showed that bulk resistance R_b decreases with increased ZrO_2 content and the intercept found for 8% ZrO_2 was the least and reverse trend was observed for 10 wt.% of ZrO_2 salt. Fig. 5b represents the complex impedance plot of the highest conducting composition (8% ZrO_2) at different levels of temperatures. As the temperature takes higher positions, the intercept is shifting towards the origin on the *x*-axis, indicating the decrease of R_b values.

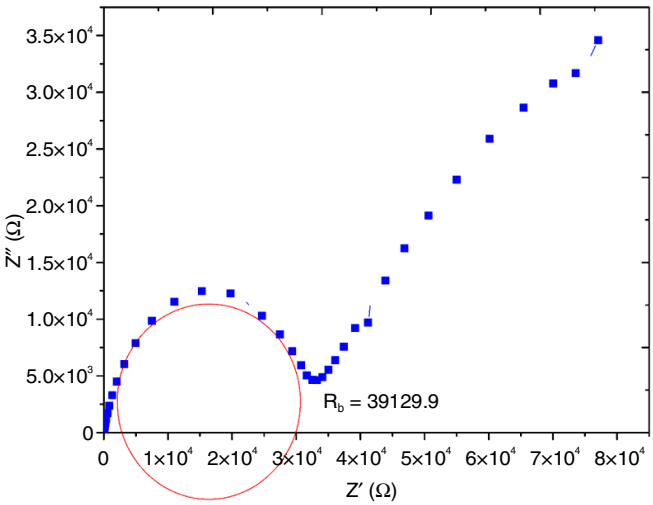

Fig. 6. R_b value calculation from Cole-Cole graph of the PVDF-*co*-HFP/$MgTf_3$/ZrO_2 (8%)

DC ionic conductivity: The DC ionic conductivity of the blend polymer electrolyte systems have been evaluated by the following formula [20]:

$$\sigma_{dc} = \frac{R_b}{t \times A} \quad (1)$$

where A is the area of cross-section, t is the thickness and R_b is the bulk resistance of the electrolyte.

The values of R_b reduced as the concentration increased. The increase of DC conductivity with concentration can be ascribed to be the dissociation of ions and thus increase the number of charge carriers [21]. The conductivity enlarges as the nanofiller ZrO_2 wt% increases [22] and highest conductivity was noticed for [(PVDF-*co*-HFP/$MgTf_3$/ZrO_2) (70/30/8%)], which could be attributed to the hopping phenomenon [23,24] between the coordination sites and polymer segmentation at 303 K. The thermal transitions observed (Fig. 7) can incorporate chain rearrangement, dielectric relaxations or melt of crystalline domains formed by the PVDF-*co*-HFP/$MgTf_3$/ZrO_2 chains in two crosslinking sites. Moreover, the activation energy (E_a) enlarges with a rise in the salt concentration, is attributed due to the formation of ion pairs and increased viscosity of the polymer matrix. Hence, the higher ambient temperature level conductivity values of PVDF-*co*-HFP/$MgTf_3$/ZrO_2 samples of electrolytes are predominantly connected with high the ionic mobility.

AC conductivity: The logarithmic conductivity plots as a difference of frequency for different polymer ratio compositions of PVDF-*co*-HFP/$MgTf_3$/ZrO_2 are shown in Fig. 8. A

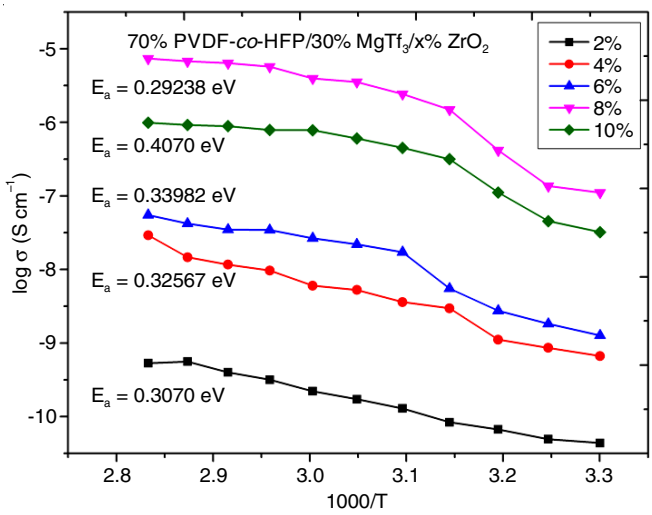

Fig. 7. Temperature dependent ionic conductivity of PVDF-*co*-HFP/$MgTf_3$/ZrO_2 with different wt% of ZrO_2 nano powder and its activation energy (E_a)

change of conductivity was due to the quick enhancement of charge carrier mobility in the complex polymer film. Generally, the frequency-dependent conductivity could exhibit in three types of dispersion regions with frequency, (i) low-frequency region, which demonstrates the space charge polarization, (ii) DC saturation zone in mid-frequency region and (iii) dc-to-ac switching at high frequency-zone, which due to the coulombic interaction of charge carrier and disruption within the framework [25,26]. Fig. 8a demonstrates the variation dependent AC conductivity of ZrO_2 nanofiller dispersed in PVDF-*co*-HFP/$MgTf_3$/ZrO_2 membrane. In general, the electrical conductivity is mainly due to the migration of Mg^{2+} present in electrolyte film. Under the influence of applied field, the charges can migrate and lead to contribute the electrical response. The frequency dependent conductivity generally follows Jonscher's power law [27,28]:

$$\sigma_{ac}(\omega) = \sigma\,\omega_0 + A\omega^n \quad (2)$$

where $\sigma_{ac}(\omega)$ is the total conductivity at a particular frequency, $\sigma\,\omega_0$ is the dc conductivity at zero frequency, ω^n is the angular frequency with A as constant, infers the polarization strength (ω) and n is the frequency exponent. Fig. 8b depicts the variation dependent AC conductivity of ZrO_2 nanofiller at different temperatures. The AC conductivity increases with increasing frequency due to increase in the ratio of successful to unsuccessful hopping. The successful hopping occurs when the neighbourhood ions became relaxed with respect to the hopping ions position and the hopping ions stay in the new site and unsuccessful hopping occurs if hopping ions jump back to its initial position [29,30].

Electric modulus: The reciprocal of complex permittivity is coined an electrical modulus. It is practiced to study space charge dielectric relaxation, the contribution of the electrode polarization consequence and the electrical conduction mechanism. From electric modulus we can also examine dielectric reaction from ion relaxation where the electrode polarization gets subdued at which frequency region. The relation between impedance *versus* M′ & M″ is shown below:

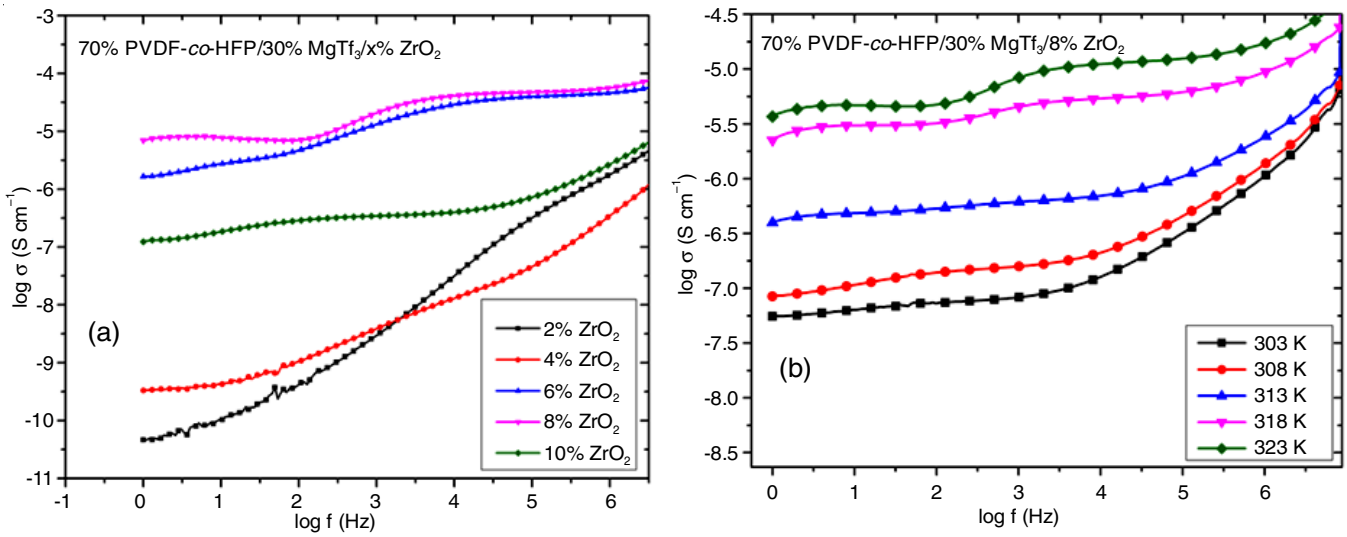

Fig. 8. Frequency dependent conductivity of (a) 70%PVDF-*co*-HFP/30%$MgTf_3$/ZrO_2 (X%) ZrO_2 (X = 2, 4, 6, 8, 10) at 303 K, (b) 70%PVDF-*co*-HFP/30%$MgTf_3$/ZrO_2 (8%) at different temperatures

$$M' = \omega C_0 Z'' \quad (3)$$

$$M'' = \omega C_0 Z' \quad (4)$$

Figs. 9 and 10 manifest the frequency-dependence of real and imaginary portions reacting to M′ and M″ of the plot of electrical modulus. The data points of M′ cluster in the low-frequency range, indicating a large capacitance linked to the electrodes that facilitates the conduction of Mg^{2+} ions [31].

From Fig. 10a, it is seen that the M″ values for 70%PVDF-*co*-HFP/30%$MgTf_3$/ZrO_2 (x%), the conductivity relaxation peaks appear. It is also observed that a shift of peak position to the higher frequency region with increase in the concentration of ZrO_2 nanopowder. It is observed that M′ value increases non-linearly with increase in frequency from 1Hz–10 MHz for NCPE films with different concentration of ZrO_2 and its M″ spectra exhibit conductivity relaxation peaks in the low frequency area. But he M′ and M″ almost remain zero in low frequency region and increases non-linearly in high frequency region [32,33]. A dispersion in PVDF-*co*-HFP/$MgTf_3$/ZrO_2 membranes was observed at high frequency region where as at low frequency region (Fig. 10b), these membranes are not indicating any dispersion in the polymer membrane. In the low frequency region, the electronic polarization results is dominated and therefore M′ and M″ values are observed closer to zero.

The imaginary modulus, M″ spectra of the ion conducting electrolyte indicates a peak in the high frequency area relating to the ionic conductivity relaxation process [34]. But, in regard of 70% PVDF-*co*-HFP/30%$MgTf_3$/ZrO_2 (8%) electrolyte system, the peaks in the M′ spectra does not exist in the scaled upper limit of the frequency range. With an increase of temperature of the membrane, the M′ and M″ dispersion have shifted toward higher frequency side, which depicts that the ionic conduction relaxation is thermally activated with the hopping of charge carriers.

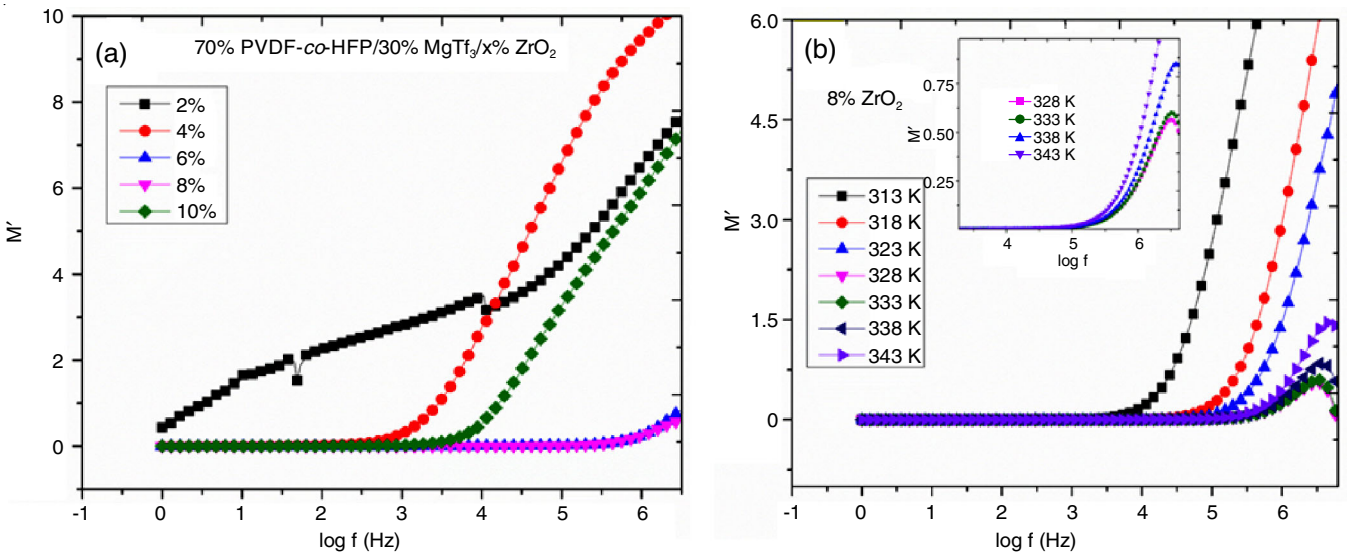

Fig. 9. Variation of real Electric modulus of (A) 70%PVDF-*co*-HFP/30%$MgTf_3$/ZrO_2 (X%) ZrO_2 (X = 2, 4, 6, 8, 10) at 303 K, (B) 70% PVDF-*co*-HFP/30%$MgTf_3$/ZrO_2 (8%) at various levels temperature

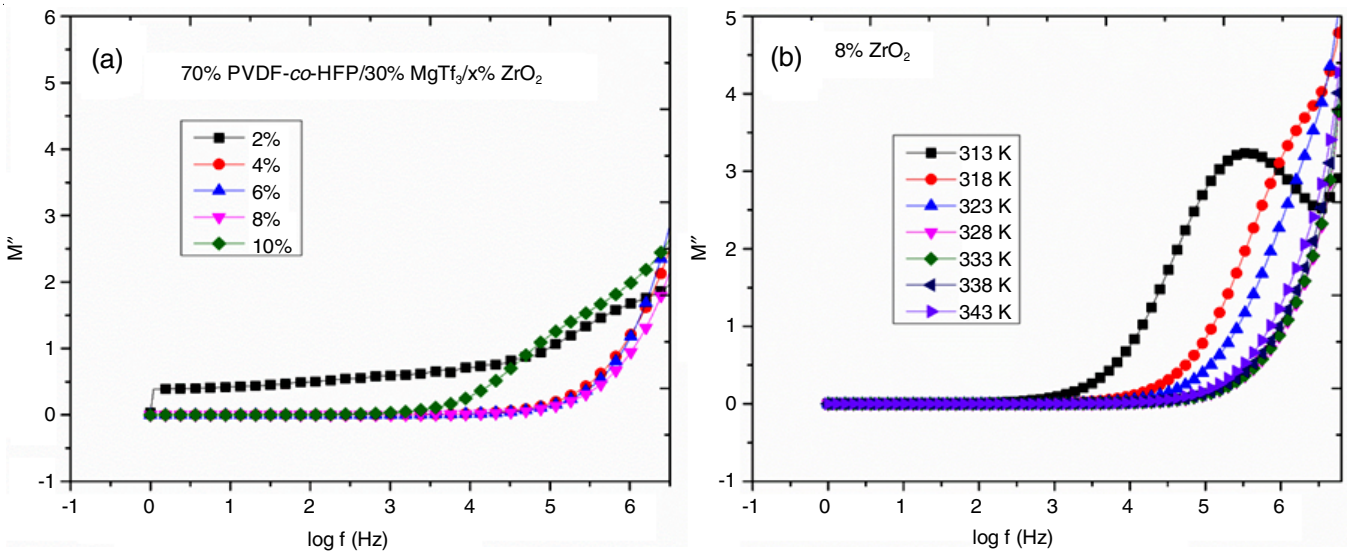

Fig. 10. Variation of imaginary Electric modulus of (A) 70%PVDF-*co*-HFP/30%$MgTf_3/ZrO_2$ (X%) ZrO_2 (X = 2, 4, 6, 8, 10) at 303 K, (B) 70% PVDF-*co*-HFP/30%$MgTf_3/ZrO_2$ (8%) at varied temperatures

Concentration dependent conductivity: It is observed that the nanocomposite polymer electrolyte with 8 wt.% nano ZrO_2 (Fig. 11). The increase in conductivity is due to the presence of nanofiller facilitating the path for the polymer segmental motion and ion transport. On further increase of nanofiller concentration, conductivity decreases. This could be due to the presence of excessive fillers in the solid polymer electrolyte may lead to the ion pairs and their aggregation inhibiting the ionic conduction and decrease in its mobility in the amorphous phase.

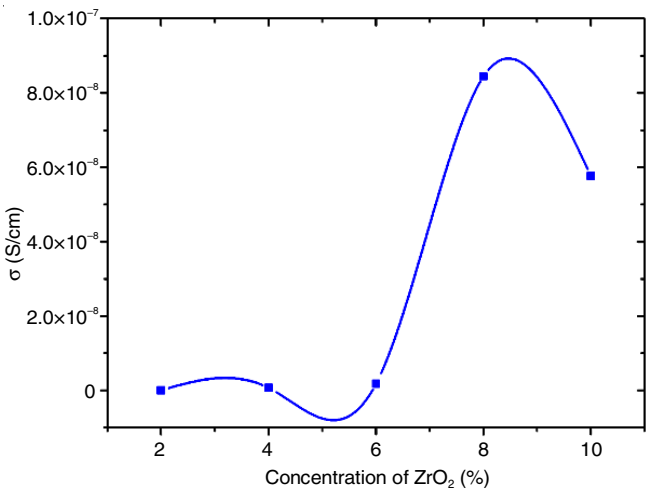

Fig. 11. Variation in conductivity 70%PVDF-*co*-HFP/30%$MgTf_3/ZrO_2$ (X%) ZrO_2 (X = 2, 4, 6, 8, 10) at 303 K

Dielectric studies: The relaxation reaction of the polymer composite (dielectric medium) to the outer electric field of microwave frequencies is said in terms of dielectric permittivity (ε^*) as mentioned below:

$$\varepsilon^* = \varepsilon'(\omega) + j\varepsilon''(\omega) \quad (5)$$

It contains real part (ε'-dielectric constant) and imaginary part (ε''-dielectric loss).

The effect of doping on increasing the frequency of charge carriers in PVDF-*co*-HFP/$MgTf_3/ZrO_2$ membranes is demonstrated by the fact that application of an electric field causes a change in the polarisation of dipoles, which in turn increases a rise in the dielectric constant.

The dielectric properties of PVDF-*co*-HFP/$MgTf_3/ZrO_2$ nanocomposite polymer membranes were observed as a function of frequency ranging from 1 Hz-35 MHz. The ε' and ε'' values of the membranes observe to scale-down with arise in frequency and attains a constant value when the frequency reaches to 10 MHz. The Koop's theory can explain this observation, that is the polycrystalline material consists of grains and grain boundaries, with the former being less resistive than the latter. When a material is subjected to an alternating electric field, charge carriers penchantmass to accumulate at the grain boundary interfaces, resulting in the formation of dipoles [35]. Because of the high resistive nature, at low frequency more charges in the composite membranes are trapped at the interfaces that results to space chargepolarization, affecting the ε' and ε'' values to be high. If the frequency amplifies, charge carriers accumulate least at the interfaces and tends to descale in the ε' and ε'' values. Such a process is called anomalous dielectric dispersion. When PVDF-*co*-HFP/$MgTf_3/ZrO_2$ membranes are compared PVDF-*co*-HFP/30%$MgTf_3/ZrO_2$ film possess lower ε' value. As the concentration of nanofiller increases the ε' value also increases that leads to interfacial polarization. Similarly ε'' value also lessens as the frequency increases. Because electric dipoles have more time to align themselves in the field direction at low frequencies, thus, the resulting e^2 values tend to be higher [36,37].

The dielectric constant rises tremendously with a rise in level of temperature because of the improvement in the contribution of ionic movability and polarization consequences. Fig. 12a clearly depicts as the level of temperature increases and charge carriers are activated and facilitates its orientation. The dielectric constant shows maximum for PVDF-*co*-HFP/$MgTf_3$/

ZrO_2 (8%) at 333 K composite. Fig. 12b indicates the frequency relying of dielectric loss at various levels of temperatures. The ε″ also rises greatly with rise in temperature. The scaling up in the temperature leads to rise in the viscosity of membrane, which enhances the friction of the revolving dipoles and degree of dipole orientation. Comparison of 70%PVDF-*co*-HFP/30% $MgTf_3$/X%ZrO_2 (X% = 2, 4, 6, 8, 10) composites revealed an increment of the dielectric properties for 8% of ZrO_2. This increment is attributed to the interaction between PVDF-*co*-HFP/$MgTf_3$/ZrO_2 matrixes. This interplay also improves the conducting pathways in the polymer matrix resulting in the tremendous increase in the mobility of Mg^{2+} ions.

Loss tangent: Using impedance analysis, dielectric loss tangent (tan δ) was calculated using the following eqns:

$$\tan \delta = Z_r Z_i \quad (6)$$

$$\tan \delta = \frac{\varepsilon_i}{\varepsilon_r} \quad (7)$$

All the tan δ of PVDF-*co*-HFP/$MgTf_3$/ZrO_2 depict a peak at the specific frequency (Fig. 13), which a comprises of a single peak indication ion conduction through the polymer segmental movement. The relaxation peaks were shifted towards the high frequency by increasing the concentration of nanofiller, resulting in the lowering of relaxation time, which may be attributed due to the different weight composition of ZrO_2 between (4-10%) may be affected by equivalence between dissolution of salt in the amorphous phase (Table-1). From Fig. 13b, it is observed that tan δ values increased with the frequency at low frequency area, since the effect of more active component (ohmic) is greater than the reactive component (capacitive). But at greater frequency, tan δ behaves in the other way round pattern due to the independence ohmic portion as the reactive component gets larger with the frequency [38]. The changing of peaks positions towards greater frequency shows the decline of relaxation time that leads to augment in charge transfer dynamics (Table-2). As the temperature increases, the relaxation time is

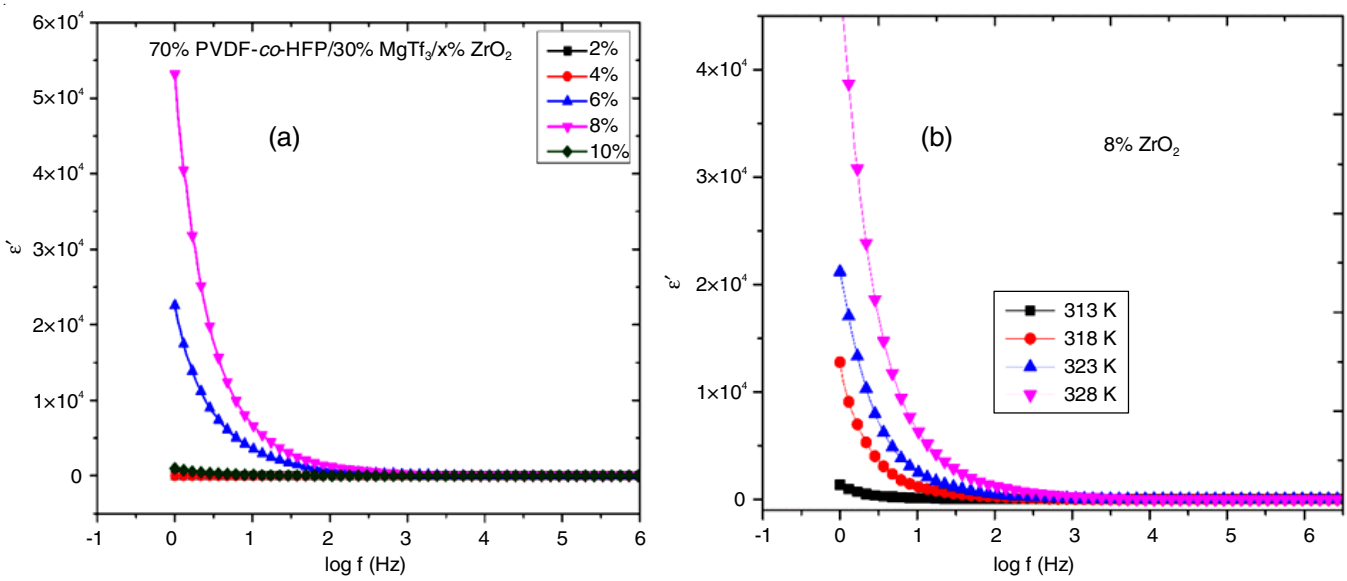

Fig. 12. Variation of Dielectric constant (A) 70%PVDF-*co*-HFP/30%$MgTf_3$/ZrO_2 (X%) (X = 2, 4, 6, 8, 10) at 303 K, (B) 70% PVDF-*co*-HFP/30%$MgTf_3$/ZrO_2 (8%) at different temperatures

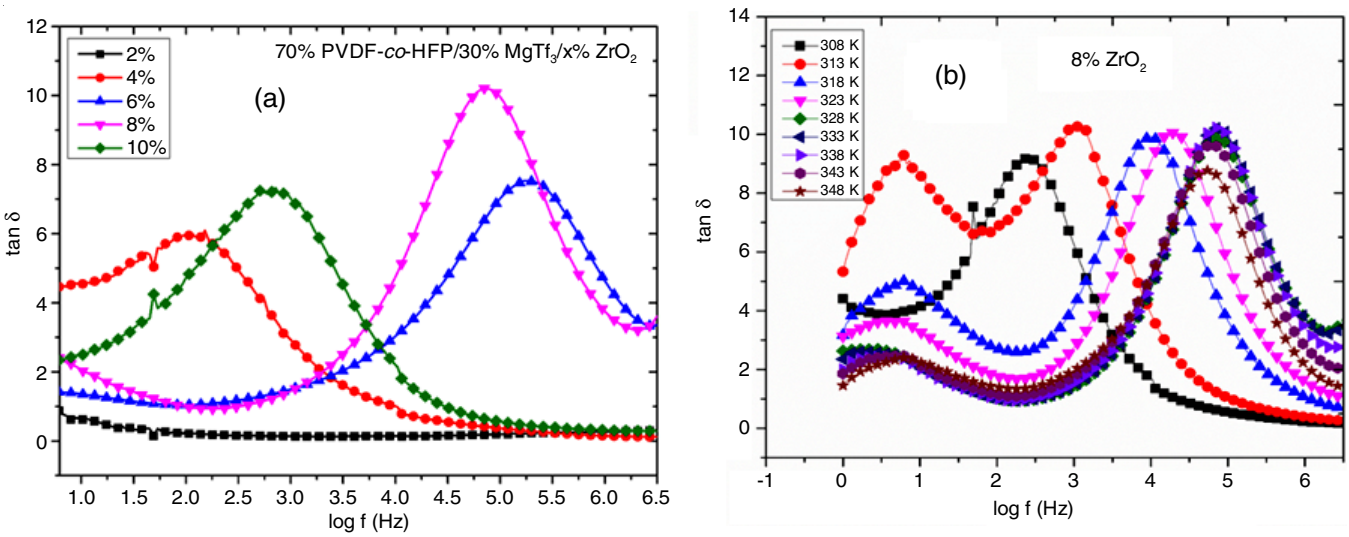

Fig. 13. (a) Frequency dependent loss tangent of $MgTf_3$ dispersed PVDF-*co*-HFP/$MgTf_3$, (b) Loss tangent of 8% ZrO_2 at different temperatures

TABLE-1
VARIATION OF tan δ, ION DIFFUSIVITY, MOBILITY, TRANSPORT NUMBER AND FREE ION DENSITY OF PVDF-*co*-HFP/$MgTf_3$/ZrO_2 MEMBRANES δ_{max} FOR DIFFERENT ZrO_2 CONCENTRATIONS

Sample	tan δ	f-max	Diffusion	n	Mu
2	1.27	0.000244184	8.54E-11	57132983542	0.009344
4	5.93	8.55596E-06	3.12E-10	5.95921E+12	0.000327
6	7.508	0.000578835	1.25E-09	3.53451E+11	0.022149
8	10.24	0.001048415	7.19E-08	1.11939E+13	0.040117
10	7.26	0.000930038	5.53E-09	9.71392E+11	0.035588

TABLE-2
RELAXATION TIME, DC IONIC CONDUCTIVITY, ACTIVATION ENERGY AND DIELECTRIC CONSTANT OF PVDF-*co*-HFP/$MgTf_3$/ZrO_2 MEMBRANES

Sample	f-max	τ (relaxation time)	DC cond.	E_a	E′
2	0.000244	0.000383368	8.54E-11	0.30700 eV	27.4
4	8.56E-06	1.34329E-05	3.12E-10	0.32567 eV	87.3
6	0.000579	0.000908772	1.25E-09	0.33982 eV	2712.9
8	0.001048	0.001646011	7.19E-08	0.29238 eV	5049.9
10	0.000930	0.001460159	5.53E-09	0.40700 eV	194.9

shifted towards high frequency until optimum temperature, which is the most efficient charge transport. After the optimum temperature, the relaxation peaks shifted towards low frequency and increase relaxation time caused by the decrease of space charge [39].

It has been observed that Z″ and M″ will not coincide at the same frequency level, Z″ expanded in lower frequency while M″ spectrum expanded in higher frequency, which stipulates the dispersion of relaxation time, *i.e.* non-Debye activity of the electrolyte films (Fig. 14).

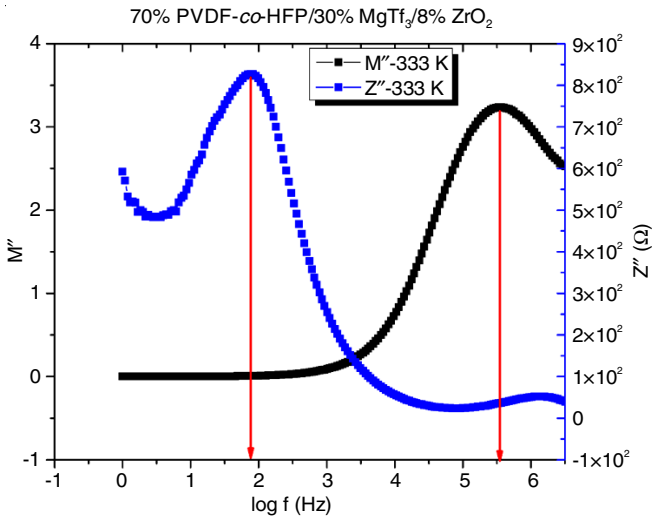

Fig. 14. Difference of Z″ and M″ of 70% PVDF-*co*-HFP/30%$MgTf_3$/ZrO_2 (8%)electrolyte membrane with frequency at 333 K

Conclusion

In the current investigation, ZrO_2 nanoparticles used as an inorganic filler in the preparation of PVDF-*co*-HFP/$MgTf_3$ membranes, which were effective in reducing the pore size and boosting the amorphous character of the membranes. It was determined that ZrO_2 nanoparticles doped with PVDF-*co*-HFP/$MgTf_3$ were complexed with PVDF-*co*-HFP and that the ZrO_2 nanoparticles transitioned from a semi-crystalline phase to an amorphous phase by FTIR measurement. The surface and porous nature of the prepared PVDF-*co*-HFP/$MgTf_3$/ZrO_2 membranes were revealed using SEM morphology. The XRD results revealed that the addition of ZrO_2 nanopowder to PVDF-*co*-HFP/$MgTf_3$ membranes, increases the amorphous region up to 8% and thereafter decreased. The glass transition and melting temperatures of ZrO_2 nanopowder embedded PVDF-*co*-HFP/$MgTf_3$ membranes, were validated using DSC analysis. The electrical and dielectric parameters confirmed the structural improvement of the polymer membrane electrolyte materials. It was revealed that 8% nanofiller is the optimal conducting composition due to the largest increase in ionic conductivity, dielectric constant and maximum movability of Mg^{2+} ions. The integration of ZrO_2 nanofiller mostly enlarges the number of most free ions and movability of PVDF-*co*-HFP/$MgTf_3$/ZrO_2 in the composite polymer electrolyte systems.

CONFLICT OF INTEREST

The authors declare that there is no conflict of interests regarding the publication of this article.

REFERENCES

1. J.B. Goodenough and K.-S. Park, *J. Am. Chem. Soc.*, **135**, 1167 (2013); https://doi.org/10.1021/ja3091438
2. S. Dühnen, J. Betz, M. Kolek, R. Schmuch, M. Winter and T. Placke, *Small Methods*, **4**, 2000039 (2020); https://doi.org/10.1002/smtd.202000039
3. L. Zhang, X. Li, M. Yang and W. Chen, *Energy Storage Mater.*, **41**, 522 (2021); https://doi.org/10.1016/j.ensm.2021.06.033
4. N. Mittal, A. Ojanguren, N. Cavasin, E. Lizundia and M. Niederberger, *Adv. Funct. Mater.*, **31**, 2101827 (2021); https://doi.org/10.1002/adfm.202101827
5. G. Foran, D. Mankovsky, N. Verdier, D. Lepage, A. Prébé, D. Aymé-Perrot and Mickaël Dollé, *iScience*, **23**, 101597 (2020); https://doi.org/10.1016/j.isci.2020.101597
6. I. Osada, H. de Vries, B. Scrosati and S. Passerini, *Angew. Chem. Int. Ed.*, **55**, 500 (2016); https://doi.org/10.1002/anie.201504971
7. K.S. Ngai, S. Ramesh, K. Ramesh and J.C. Juan, *Ionics*, **22**, 1259 (2016); https://doi.org/10.1007/s11581-016-1756-4

8. V.S. Voet, G. ten Brinke and K. Loos, *J. Polym. Sci. A Polym. Chem.*, **52**, 2861 (2014); https://doi.org/10.1002/pola.27340
9. Z. Qiu, X. Liu, J.W. Lam and B.Z. Tang, *Macromol. Rapid Commun.*, **40**, 1800568 (2019); https://doi.org/10.1002/marc.201800568
10. Y. Xia, X. Wang, X. Xia, R. Xu, S. Zhang, J. Wu, Y. Liang, C. Gu and J. Tu, *Chem. Eur. J.*, **23**, 15203 (2017); https://doi.org/10.1002/chem.201703464
11. J. Shi, Y. Yang and H. Shao, *J. Membr. Sci.*, **547**, 1 (2018); https://doi.org/10.1016/j.memsci.2017.10.033
12. R. Prasanth, N. Shubha, H.H. Hng and M. Srinivasan, *Eur. Polym. J.*, **49**, 307 (2013); https://doi.org/10.1016/j.eurpolymj.2012.10.033
13. M.F. Bósquez-Cáceres, S. Hidalgo-Bonilla, V. Morera Córdova, R.M. Michell and J.P. Tafur, *Polymers*, **13**, 4284 (2021); https://doi.org/10.3390/polym13244284
14. J. Hu, W. Wang, B. Zhou, Y. Feng, X. Xie and Z. Xue, *J. Membr. Sci.*, **575**, 200 (2019); https://doi.org/10.1016/j.memsci.2019.01.025
15. A. Das, N.T. Balakrishnan, N.S. Jishnu, J.D. Joyner, J.H. Ahn, F.M. Jabeen and P. Raghavan, Eds.: P. Raghavan and M.J. Jabeen Fatima, In Polymer Electrolytes for Energy Storage Devices, CRC Press, pp. 133-148 (2021).
16. K. Mishra, T. Arif, R. Kumar and D. Kumar, *J. Solid State Electrochem.*, **23**, 2401 (2019); https://doi.org/10.1007/s10008-019-04348-9
17. I.K. Sani, S.P. Geshlaghi, S. Pirsa and A. Asdagh, *Food Hydrocoll.*, **117**, 106719 (2021); https://doi.org/10.1016/j.foodhyd.2021.106719
18. W. Zheng, L. Ren, X. Zhao, C. Wang, L. Yang and R. Liao, *Molecules*, **27**, 4289 (2022); https://doi.org/10.3390/molecules27134289
19. P. Sharma, D.K. Kanchan and N. Gondaliya, *Open J. Org. Polym. Mater.*, **2**, 38 (2012); https://doi.org/10.4236/ojopm.2012.22006
20. P. Dhatarwal and R. J. Sengwa, *SN Appl. Sci.*, **2**, 833 (2020); https://doi.org/10.1007/s42452-020-2656-9
21. S. Karthikeyan, S. Sikkanthar, S. Selvasekarapandian, D. Arunkumar, H. Nithya and J. Kawamura, *J. Polym. Res.*, **23**, 51 (2016); https://doi.org/10.1007/s10965-016-0952-2
22. P. Shanmugaraj, A. Swaminathan, R.K. Ravi, M. Dasaiah, P. Senthil Kumar and A. Sakunthala, *J. Mater. Sci. Mater. Electron.*, **30**, 20079 (2019); https://doi.org/10.1007/s10854-019-02380-z
23. K. Kiran Kumar, M. Ravi, Y. Pavani, S. Bhavani, A.K. Sharma and V.V.R. Narasimha Rao, *J. Non-Cryst. Solids*, **358**, 3205 (2012); https://doi.org/10.1016/j.jnoncrysol.2012.08.022
24. D.K. Pradhan, R.N.P. Choudhary and B.K. Samantaray, *Int. J. Electrochem. Sci.*, **3**, 597 (2008).
25. A. Arya and A.L. Sharma, *Ionics*, **25**, 1617 (2019); https://doi.org/10.1007/s11581-019-02916-7
26. R. Manjuladevi, M. Thamilselvan, S. Selvasekarapandian, R. Mangalam, M. Premalatha and S. Monisha, *Solid State Ion.*, **308**, 90 (2017); https://doi.org/10.1016/j.ssi.2017.06.002
27. H.M. Zaki, *Physica B*, **363**, 232 (2005); https://doi.org/10.1016/j.physb.2005.03.026
28. S. Ibrahim, S.M. Mohd Yasin, N.M. Nee, R. Ahmad and M.R. Johan, *Solid State Commun.*, **152**, 426 (2012); https://doi.org/10.1016/j.ssc.2011.11.037
29. M.B. Hossena and A.K.M. Akther Hossain, *J. Adv. Ceram.*, **4**, 217 (2015); https://doi.org/10.1007/s40145-015-0152-2
30. R.J. Sengwa, P. Dhatarwal and S. Choudhary, *Solid State Ion.*, **324**, 247 (2018); https://doi.org/10.1016/j.ssi.2018.07.015
31. J.S. Kim, *J. Phys. Soc. Jpn.*, **70**, 3129 (2001); https://doi.org/10.1143/JPSJ.70.3129
32. N. Kulshrestha, B. Chatterjee and P.N. Gupta, *High Perform. Polym.*, **26**, 677 (2014); https://doi.org/10.1177/0954008314541820
33. K.P. Singh and P.N. Gupta, *Eur. Polym. J.*, **34**, 1023 (1998); https://doi.org/10.1016/S0014-3057(97)00207-3
34. Y. Yang, J. He, G. Wu and J. Hu, *Sci. Rep.*, **5**, 16986 (2015); https://doi.org/10.1038/srep16986
35. R. Baskaran, S. Selvasekarapandian, G. Hirankumar and M.S. Bhuvaneswari, *Ionics*, **10**, 129 (2004); https://doi.org/10.1007/BF02410321
36. S.A. Wahab, M. Ahmed, F. Radwan, R. Hassan and A. El-Refae, *Mater. Lett.*, **30**, 183 (1997); https://doi.org/10.1016/S0167-577X(96)00196-6
37. K.S. Ngai, S. Ramesh, K. Ramesh and J.C. Juan, *Chem. Phys. Lett.*, **692**, 19 (2018); https://doi.org/10.1016/j.cplett.2017.11.042
38. K. Nakamura, T. Saiwaki and K. Fukao, *Macromolecules*, **43**, 6092 (2010); https://doi.org/10.1021/ma100918e
39. S. Chopra, S. Sharma, T.C. Goel and R.G. Mendiratta, *Solid State Commun.*, **127**, 299 (2003); https://doi.org/10.1016/S0038-1098(03)00431-9